XVIII IMEKO WORLD CONGRESS
Metrology for a Sustainable Development
September, 17–22, 2006, Rio de Janeiro, Brazil

ULTRASOUND MICROSCOPY TECHNIQUES TO DETECT DELAMINATION IN STACKED LAYERS

Stefan Johann Rupitsch[1], *Bernhard Günther Zagar*[2]

[1]Institute for Measurement Technology, Linz, Austria, stefan.rupitsch@jku.at
[2]Institute for Measurement Technology, Linz, Austria, bernhard.zagar@jku.at

Abstract: We present the theory and some applications of the synthetic aperture focusing technique applied to single transducer ultrasonic data sets. In this technique a virtual source located at the geometrical focal point of the physical transducer is algorithmically generated and thus allows for tighter focusing over a geometrically larger scan volume. We present results from a structural test phantom (two copper wires) and a delaminated specimen.

Keywords: ultrasound, synthetic aperture focusing technique, virtual source, B–mode imaging, delamination.

1. INTRODUCTION

Ultrasonic imaging is widely used in the material testing where different scanning schemes are employed. The main disadvantage of common B–mode imaging lies in the depth dependent lateral resolution in the image. The synthetic aperture focusing technique (SAFT) overcomes this principle limitation [1, 2]. The SAFT treats the transducer's focal point as a virtual source generating spherical waves over a certain aperture angle. With SAFT a depth–independent resolution within certain limits (actually diffraction limited) is achieved theoretically.

In this paper we use a transducer with a fixed focus, that is laterally displaced to yield structural information of an object. Subsequently an off line SAFT–algorithm is applied to the already recorded echo–signals for each scan line resulting in an enhanced B–mode image.

Experiments with a pair of 180 μm copper wires are performed to evaluate the imaging quality of the synthetic aperture focusing technique. The wires were placed in the positive and negative defocus regions. We present the applicability of preliminary experimental data for the location of delamination in stacked material layers. As a test specimen two transparent Perspex plates are stuck together and the adhesive joint is investigated.

2. THEORETICAL DERIVATIONS

2.1. Principle of synthetic aperture imaging with a virtual source element

The synthetic aperture technique considers the transducers focal point as a virtual source (Fig. 1), which is assumed to produce a pressure wave. Its pressure wave is spherical within a certain angular extend 2Θ and propagates in both the forward and backward direction with respect to the transducer. Displacing of the transducer in positive or negative x–direction by sufficiently small increments Δx cause an overlapping field generated by the virtual sources, where the synthetic aperture focusing can be performed. One can see, that the desired focal point P in Fig. 1 is exposed to the virtual source's fields at the lateral position x_0 and $x_i = x_0 + i\Delta x$ $(i = \pm 1, \pm 2 \ldots)$.

With the aim of evaluating the synthetic aperture for a desired focal point P all transducer echo signals from different lateral position x_i, which cause a field in P are summed up coherently. Due to the different transducer positions and therefore different distances from the virtual sources to the desired focal point P time delays Δt_i occur. Note that these time delays need to be calculated to obtain coherent summation. The time delay Δt_i is given by

$$\Delta t_i = \frac{2\,(d_i - d_0)}{c} \operatorname{sgn}\{z - z_0\}\ , \tag{1}$$

where $x_i - x_0 = i\Delta x$ denotes the lateral transducer displacement, c is the propagation velocity of the acoustic wave, z_0 stands for the geometrical focal depth of the ultrasonic transducer, z is depth of the desired focal point P, d_i describes the distance from the virtual source to P at the lateral position x_i and $d_0 = \operatorname{abs}(z - z_0)$ is the axial distance from point P to the virtual source. d_i can be expressed as

$$d_i = \sqrt{d_0^2 + (i\Delta x)^2}\ . \tag{2}$$

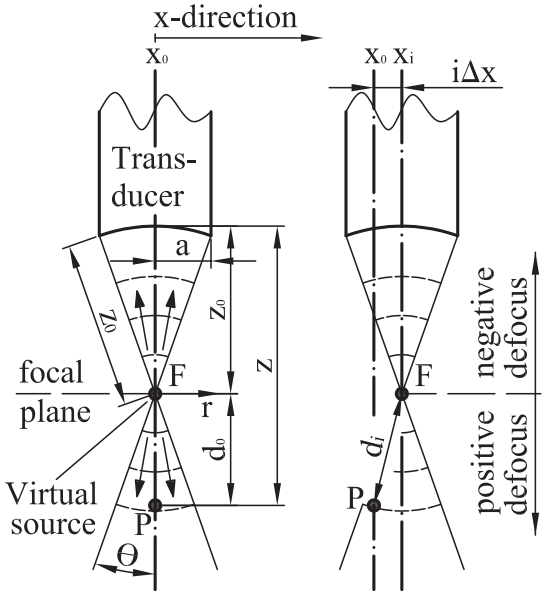

Fig. 1: Schematic of the synthetic aperture imaging using a virtual source element

The signum function in Eq. 1 is necessary to distinguish desired focal points P in the positive defocus region $(z - z_0) > 0$ from points in the negative defocus region $(z - z_0) < 0$.

$S_\Sigma(P)$, the coherently summed signal for the desired focal point P can be calculated as

$$S_\Sigma(P) = \sum_{i=-N}^{N} \alpha_i S(t_p + \Delta t_i, i) \ , \tag{3}$$

where $S(t, i)$ (common B–mode image, shown for example in Fig. 7) stands for the received two–dimensionally sampled echo signal from the lateral transducer positions x_i. $t_p = (2z)/c$ is twice of the time–of–flight of the acoustic wave in the propagation medium for the axial distance z. α_i is an apodization weight [3, 4] to suppress side lobes and is normally a function of the lateral distance. In this study a simple boxcar function is used to achieve best lateral resolution and therefore $\alpha_i = 1 \ \forall i$. N in Eq. 3 refers to the received echo signals from lateral transducer positions, which contribute to the sum and depends on the lateral spacing Δx of the transducer positions, the aperture angle 2Θ and the axial distance d_0 from the virtual source to the desired focal point. The half aperture angle Θ is defined by Eq. 4 where $2a$ is the element size of the transducer (Fig 1).

$$\Theta = \arcsin\left(\frac{a}{z_0}\right) \tag{4}$$

2.2. Lateral resolution of a spherically focused transducer

Until now it was assumed that the transducer focus is point like but strictly speaking it is really a focal volume with finite extent.

The normalized lateral acoustic pressure distribution in cylindrical coordinates of a spherically focused transducer in the focal plane ($z = z_0$) can be expressed as

$$\left|\frac{p(r)}{p_0}\right| = \left|\frac{2J_1\left(\frac{kra}{z_0}\right)}{\left(\frac{kra}{z_0}\right)}\right| \ , \tag{5}$$

with the acoustic pressure p_0 in the focal point ($r = 0$) (Fig. 1) and the wave number k. $p(r)$ denotes the acoustic pressure at distance r from the focal point in the focal plane. The operator $J_1(\cdot)$ in Eq. 5 is the Bessel–function of the first kind of order one [5, 6].

From Eq. 5 the -3 dB–lateral beam width bw_{lat} for transmit only, which is equal to the -6 dB–lateral beam width for the transmit–receive mode (used in this study) of the ultrasonic transducer in the geometrical focal plane can be calculated as

$$bw_{lat} = 1.028\left(\frac{\lambda z_0}{2a}\right) \ , \tag{6}$$

with λ the acoustic wavelength.

3. MEASUREMENT SET–UP

In Fig. 2 one can see a schematics of the measurement set–up. The specimens are placed in a tank filled with distilled and degassed water. The transducer (Panametrics V390) is spherically focused with a focal length z_0 of 12.8 mm, an element size $2a$ of 6.35 mm and an aperture angle Θ of 28.72° (Eq. 4). With the center frequency $f_c = 44.52$ MHz of the transducer, an acoustic wavelength of 33.2 μm is obtained and the -6 dB beam width results in $bw_{lat} = 68.9$ μm (Eq. 6). The transducer is excited by a pulse train generated by a Pulser/Receiver (Panametrics PR–5900), which operates in pulse/echo mode. Received signals are digitized by a 2 GSample/s oscilloscope (Tektronix TDS 744 A). The transducer is traversed in three dimensions with a translation unit driven by a motor controller (Linos x.act Commander ST3). The x– and y–positions outlined in later measurement results are always related to the reference–position of the translation unit. The whole measurement set–up is controlled by a 3.0 GHz–PC.

4. MEASUREMENT RESULTS AND DISCUSSION

The general goal of the signal processing lies in obtaining as precisely as possible the correct lateral and axial position of the targets as well as their dimension and it might also be of interest to resolve internal structures.

4.1. Structural Resolution Test Target

With the aim to determine the ultimate resolution of the current measurement system an impulse function

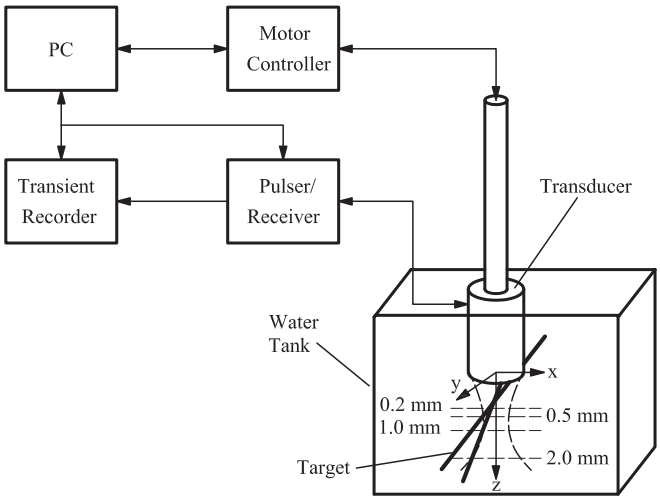

Fig. 2: Block diagram of the measurement set–up

mimicking target was devised [1, 3, 5]. It consists of two copper wires with 180 μm diameter tapering off to an intersection. So an effective and well determined lateral spacing between 0.2 mm and 2.0 mm can be selected to test spatial resolution as shown in Fig. 2 schematically. The wires were placed in both positive defocus region $z - z_0 \approx 4.2$ mm (Fig. 3) and negative defocus region $z - z_0 \approx -5.5$ mm (Fig. 4). The transducer was displaced in x–direction (lateral) and the spacing between scan lines Δx was set to 20 μm. 176 scan lines were recorded with a sampling rate of 2 GSamples/s with 1621 samples each.

The images in Fig. 3 and Fig. 4 are displayed as magnitude of the complex envelope S_H of the raw data and SAFT–processed data respectively [7].

$$S_H = |\mathcal{H}(S_O)| \tag{7}$$

The operator $\mathcal{H}(\cdot)$ in Eq. 7 stands for Hilbert–transformation, $|\cdot|$ is the absolute value, S_O is the original data set and S_H denotes the magnitude of the complex enveloped original data.

In order to extend the dynamic range in the printed images a dynamic compression is performed by applying a square root function normalized to the peak value of complex enveloped data.

The true lateral spacings of the wires were 0.2 mm (Fig. 3[a,b] and Fig. 4[a,b]), 0.5 mm (Fig. 3[c,d] and Fig. 4[c,d]), 1.0 mm (Fig. 3[e,f] and Fig. 4[e,f]) and 2.0 mm (Fig. 3[g,h] and Fig. 4[g,h]). One can observe typical hyperbolically echoes due to the lateral scanning of the transducer caused by the wires being located outside the transducer's focal point, which is in a depth of $z_0 = 12.8$ mm. Figures 3[b,d,f,h] and Figures 4[b,d,f,h] on the other hand are the SAFT–processed data corresponding to the respective raw data shown on the left. Using the SAFT–algorithm no hyperbolic reflected echoes from the wires occur anymore, which facilitate the exact localization of the two wires.

The non–ideal transducer spatial impulse response cause second order diffraction effects which are clearly visible in the box A in Fig. 3[c]. Beside artifacts they are still visible due to the square root compression in the box B in Fig. 3[d].

Another interesting fact is observable in the images. The rear reflections of the wires are positioned exactly were they geometrically are expected even though the longitudinal acoustic wave propagation velocity in copper ($c_{Cu} = 5010$ m/s) is more than three times larger than in water. This is attributed to a consequence of the Babinetsches–principle [8].

Figure 4 shows similar results for negative defocus region. It is interesting to note that artifacts are less pronounced and less visible here. Additionally the second order diffraction effects caused by the non–ideal transducer spatial impulse response are not observable in the raw data (left panels of Fig. 4) as well as in the SAFT–processed data (right panels of Fig. 4).

Furthermore faint echoes can be observed in the copper filled region. Their exact cause is to be investigated further on.

4.2. Delamination in stacked Perspex plates

With the intention to prove the efficacy of SAFT–algorithm for localization of delamination areas two optical transparent Perspex plates with a dimension of $20 \times 20 \times 4.75$ mm^3 were stuck together with a plastic glue. Due to the usage of transparent Perspex plates the glued region, which is less than 0.2 mm in thickness can be investigated both acoustically and optically.

Figure 5 is an optical image of the region of interest of the two adherent Perspex plates. An acoustic image (Fig. 6) consisting of 121×121 points in x– and y–direction was performed for the section indicated as A in Fig. 5. The grid spacing between two adjacent scan points was 25 μm in each direction. The maximum of the magnitude of the complex envelope of an A–scan was recorded with the oscilloscope and stored. The inadequately glued regions (delaminations), which are usually accompanied by trapped air bubbles cause a higher output–voltage of the pulser/receiver due to the large acoustic mismatch of Perspex and air.

In order to investigate the size and localization of the inadequately glued region a B–mode image at the fixed y–position of 56.4 mm (see Fig. 5 and Fig. 6) was generated. 251 scan lines with a lateral spacing between two adjacent scan lines of 10 μm were recorded with a sampling rate of 2 GSample/s with 541 samples each. Again the magnitude of the complex envelope (Eq. 7) is visualized in Fig. 7 as a contour–plot.

Figure 8 shows the result of the SAFT–processed raw data of Fig. 7. Note that it is of prime importance to

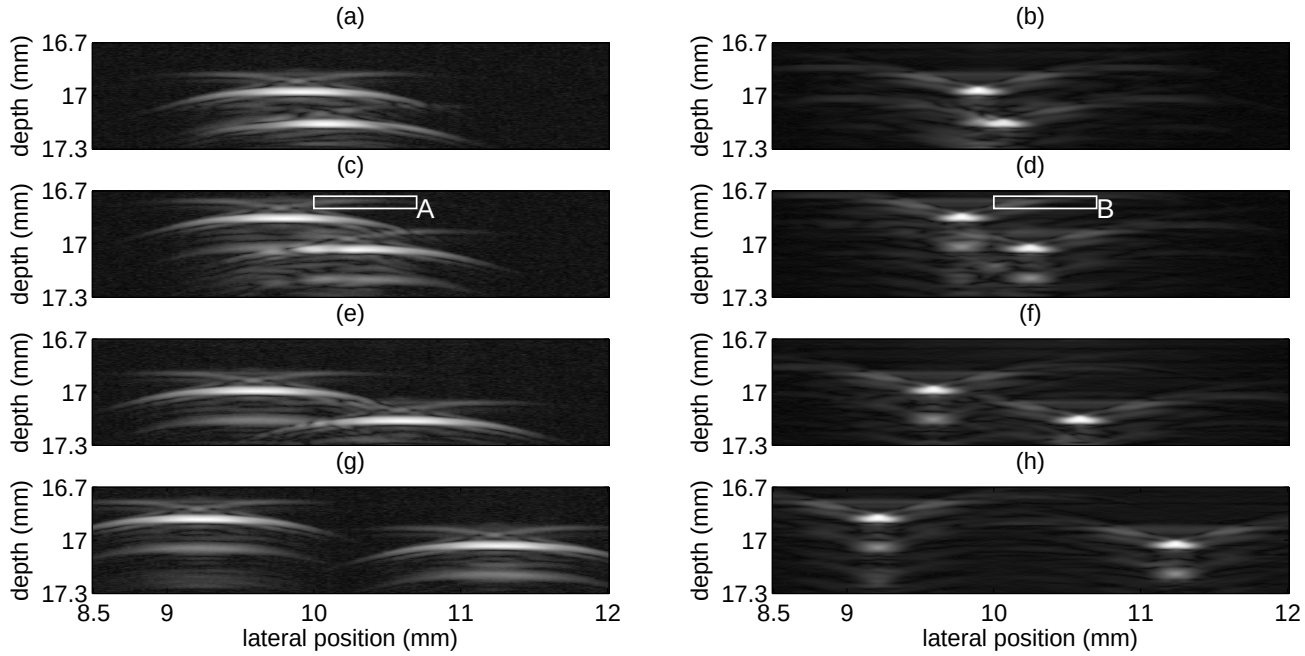

Fig. 3: The left panels show raw data dynamically compressed to visualize even weak echoes and Hilbert–transformed to get a depth averaged image of the two copper wires tapering off with a lateral spacing of 0.2 mm [(a)], 0.5 mm [(c)], 1.0 mm [(e)] and 2.0 mm [(g)] respectively. In the right panels the corresponding SAFT–processed data are shown, again dynamically compressed and Hilbert–transformed. All the images are for the positive defocus region.

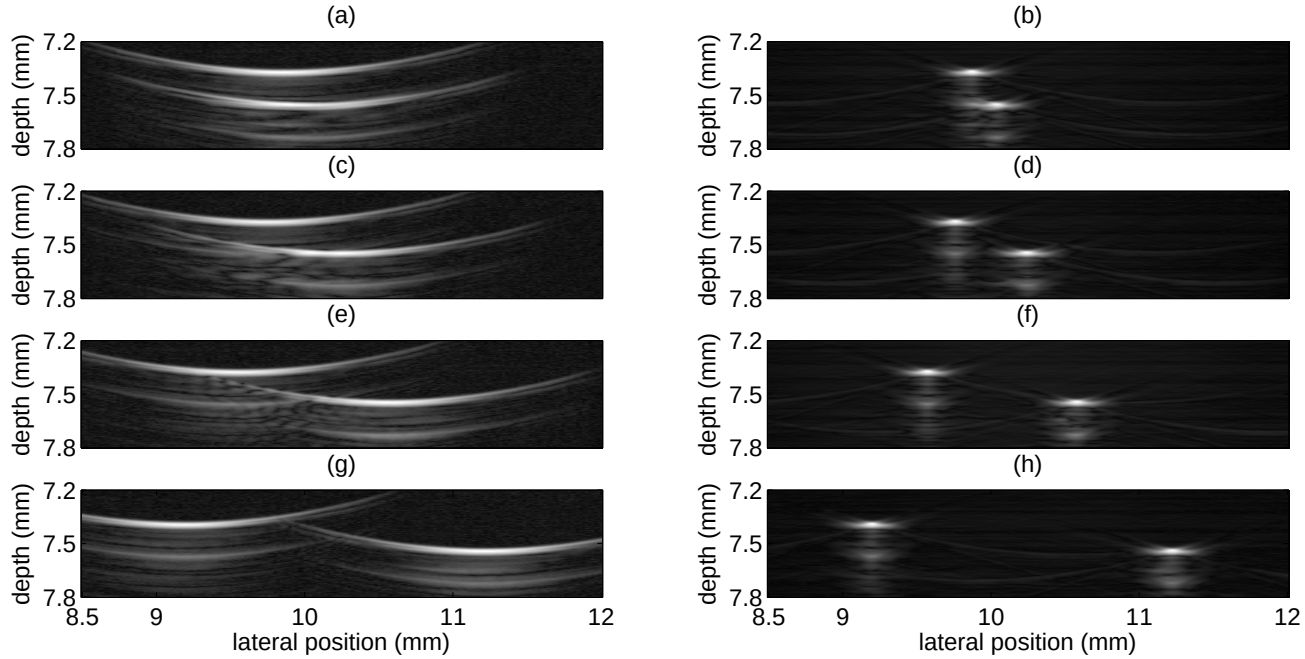

Fig. 4: The left panels show raw data dynamically compressed to visualize even weak echoes and Hilbert–transformed to get a depth averaged image of the two copper wires tapering off with a lateral spacing of 0.2 mm [(a)], 0.5 mm [(c)], 1.0 mm [(e)] and 2.0 mm [(g)] respectively. In the right panels the corresponding SAFT–processed data are shown, again dynamically compressed and Hilbert–transformed. All the images are for the negative defocus region.

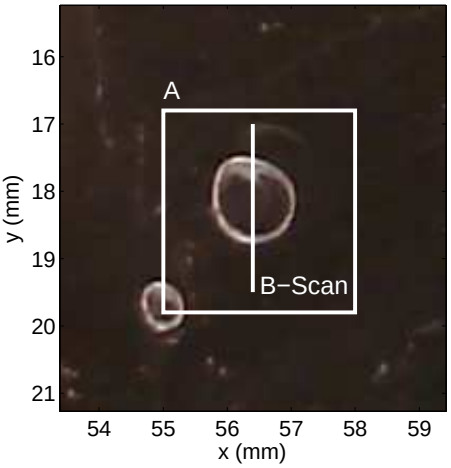

Fig. 5: Optical front view image of the region of interest of the two glued Perspex plates

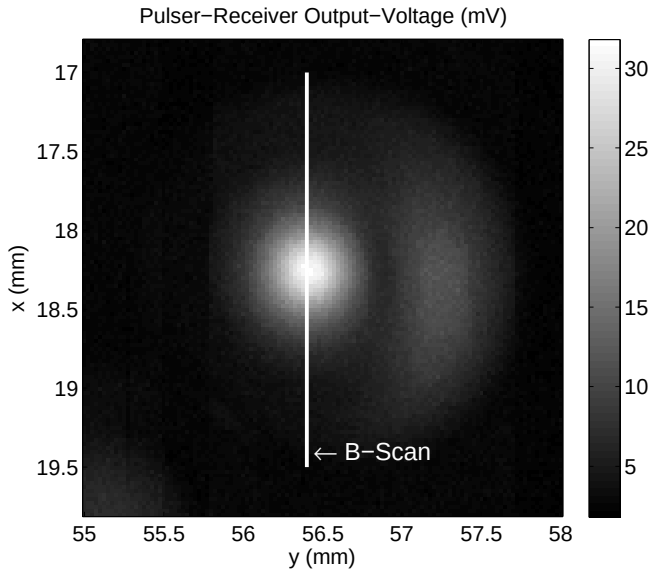

Fig. 6: Acoustic image of the zone A from Fig. 5 (121×121 points)

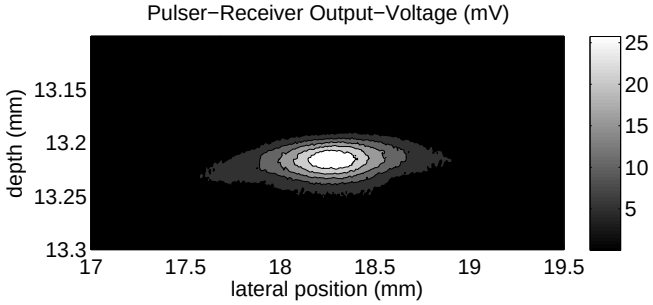

Fig. 7: Common B–mode image at the fixed y–position 56.4 mm)

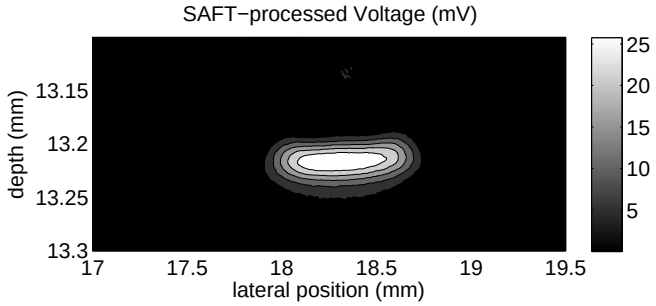

Fig. 8: B–mode image after SAFT–processing of the raw data from Fig. 7

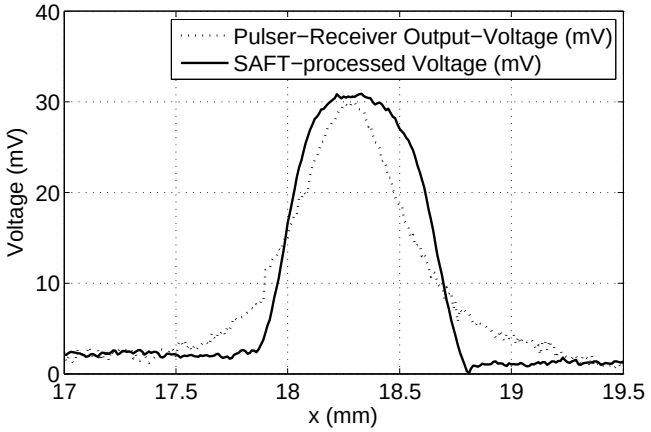

Fig. 9: Common B–mode image compared to SAFT–processed data at the fixed depth of 13.22 mm

take the different acoustic wave propagation velocity of water (c_w = 1480 m/s) and Perspex (c_p = 2700 m/s) into account to obtain the correct SAFT results.

In Fig. 9 one can see the common B–mode image and SAFT–processed image at the fixed depth of 13.22 mm. This is done with a view of comparing the common B–mode image and SAFT–processed image to the optical image. For common B–mode imaging a −6 dB object size of 0.54 mm is achieved. In contrast 0.66 mm is −6 dB object size obtained from SAFT–processed data, which is in a close agreement with the result from the optical image. Using the optical image the extension of the inadequately glued region is 0.70 mm.

5. CONCLUSIONS AND FUTURE WORK

An approach to locate layer delamination was developed. The principle of ultrasound synthetic aperture imaging using a virtual source element was applied. Experimental results were shown for a pair of 180 μm copper wires and two glued Perspex plates with inadequately glued regions to demonstrate the efficacy of the SAFT–algorithm.

Currently the presented SAFT–algorithm is applicable to material science problems like detection and location of layer delamination of printed circuit boards.

ACKNOWLEDGEMENTS

The authors greatly acknowledge the partial support of the research presented in this paper by the Linz Center of Competence in Mechatronics (LCM).

REFERENCES

[1] Stefan J. Rupitsch, Florian Maier, Bernhard G. Zagar, " Synthetic Aperture Focusing Technique in High–Frequency Ultrasound Imaging to Locate Layer Delamination", *Proc. of the IEEE IMTC–Instrumentation and Measurement Technology Conference*, 2006.

[2] C. Passmann, H. Ermert, "In Vivo Imaging of the Skin in the 100 MHz Region using the Synthetic Aperture Concept", *IEEE Ultrasonics Symposium*, 1995.

[3] Catherine H. Frazier, William D. O'Brien, "Synthetic Aperture Techniques with a virtual Source Element", *IEEE Trans. Ultrason. Freq. Contr.*, vol. 45, no 1, pp. 196–207, January 1998.

[4] Meng–Lin Li, Wei–Jung Guan, Pai–Chi Li, "Improved Synthetic Aperture Focusing Technique with Applications in High–Frequency Ultrasound Imgaging", *IEEE Trans. Ultrason. Freq. Contr.*, vol. 51, no 1, pp. 63–70, January 2004.

[5] Kay Raum, William D. O'Brien, "Pulse–Echo Field Distribution Measurement Technique for High–Frequency Ultrasound Sources", *IEEE Trans. Ultrason. Freq. Contr.*, vol. 44, no 4, pp. 810–815, July 1997.

[6] Gordon S. Kino, "Acoustic Waves, Devices, Imaging and Analog Signal Processing", *Prentice Hall*, 1987.

[7] Alan V. Oppenheim, Ronald W. Schafer, "Discrete–Time Signal Processing", Second Edition, *Prentice Hall*, 1999.

[8] Eugene Hecht, "Optics", Fourth Edition, *Benjamin Cummings*, 2003.